arXiv:0807.1189v2 [nucl-ex] 15 Jan 2009

Single-Pion Production in pp Collisions at 0.95 GeV/c (II)

S. Abd El-Samad[8], R. Bilger[6], K.-Th. Brinkmann[2], H. Clement[6], M. Dietrich[6], E. Doroshkevich[6], S. Dshemuchadse[5,2], K. Ehrhardt[6], A. Erhardt[6], W. Eyrich[3], A. Filippi[7], H. Freiesleben[2], M. Fritsch[3,1], R. Geyer[4], A. Gillitzer[4], J. Hauffe[3], D. Hesselbarth[4], R. Jaekel[2], B. Jakob[2], L. Karsch[2], K. Kilian[4], J. Kress[6], E. Kuhlmann[2], S. Marcello[7], S. Marwinski[4], R. Meier[6], K. Möller[5], H.P. Morsch[4], L. Naumann[5], J. Ritman[4], E. Roderburg[4], P. Schönmeier[2,3], M. Schulte-Wissermann[2], W. Schroeder[3], F. Stinzing[3], G.Y. Sun[2], J. Wächter[3], G.J. Wagner[6], M. Wagner[3], U. Weidlich[6], A. Wilms[1], S. Wirth[3], G. Zhang[6a], and P. Zupranski[9]

[1] Ruhr-Universität Bochum, Germany
[2] Technische Universität Dresden, Germany
[3] Friedrich-Alexander-Universität Erlangen-Nürnberg, Germany
[4] Forschungszentrum Jülich, Germany
[5] Forschungszentrum Rossendorf, Germany
[6] Physikalisches Institut der Universität Tübingen, Tübingen, Germany
[7] University of Torino and INFN, Sezione di Torino, Italy
[8] Atomic Energy Authority NRC Cairo, Egypt
[9] Soltan Institute for Nuclear Studies, Warsaw, Poland
(COSY-TOF Collaboration)

January 15, 2009

Abstract. The single-pion production reactions $pp \to d\pi^+$, $pp \to np\pi^+$ and $pp \to pp\pi^0$ were measured at a beam momentum of 0.95 GeV/c ($T_p \approx 400$ MeV) using the short version of the COSY-TOF spectrometer. The central calorimeter provided particle identification, energy determination and neutron detection in addition to time-of-flight and angle measurements from other detector parts. Thus all pion production channels were recorded with 1-4 overconstraints. The main emphasis is put on the presentation and discussion of the $np\pi^+$ channel, since the results on the other channels have already been published previously. The total and differential cross sections obtained are compared to theoretical calculations. In contrast to the $pp\pi^0$ channel we observe in the $np\pi^+$ channel a strong influence of the Δ excitation. In particular the pion angular distribution exhibits a $(3 \, cos^2\Theta + 1)$ dependence, typical for a pure s-channel Δ excitation and identical to that observed in the $d\pi^+$ channel. Since the latter is understood by a s-channel resonance in the $^1D_2$ pn partial wave, we discuss an analogous scenario for the $pn\pi^+$ channel.

PACS. 13.75.Cs – 14.20.Gk – 14.20.Pt – 25.10.+s – 25.40.Ep

1 Introduction

Single-pion production in the collision between two nucleons is thought to be the simplest inelastic process between two baryons, nevertheless its understanding is still far from being satisfactory - both from the theoretical and the experimental point of view. In a recent publication [1] – in the following denoted by (I) – we have presented the first kinematically complete measurement for the $pp \to pp\pi^0$ channel at a beam momentum of 0.95 GeV/c (corresponding to $T_p =$397 MeV). Although Δ production in a relative s-wave is prohibited in this reaction channel, we have seen that the angular distributions indi-

cate the presence of significant Δ production in a relative p-wave already close to threshold.

In this work we present our results for the $pp \to pn\pi^+$ channel at the same incident energy. We will show that here, where Δ production in relative s-wave is allowed, indeed this production process is overwhelmingly dominant and characterizes the differential observables in this channel.

The reaction of interest here has been investigated in the near-threshold region already previously by a series of measurements at JINR [2], KEK [3,4], TRIUMF [5], CELSIUS [6] and notably at IUCF [7,8,9,10], since there experiments have been carried out both with polarized beam and target. In these measurements very close to threshold it was already noted [7] that at beam energies of $T_p =$ 320 MeV, i.e. only 20 MeV above threshold, an onset of the Δ excitation is seen in the pion angular distribution.

---

[a] present address: Peking University
Correspondence to: H. Clement
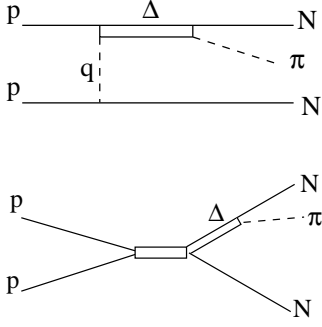email: clement@pit.physik.uni-tuebingen.de

Fig. 1. Graphs used for the theoretical calculations. Top: t-channel approach (PWIA, direct part only), bottom: s-channel approach.

The latter changes from isotropic at energies below 300 MeV to anisotropic at 320 MeV suggesting there a 30 - 40 % contribution of the Δ excitation. In the TRIUMF measurements, which were performed at beam energies of $T_p = 420$ and 500 MeV, it was noticed that at these energies the pion angular distributions of $pp \rightarrow d\pi^+$ and $pp \rightarrow pn\pi^+$ reactions are not only very similar, but also very close to the angular distribution expected from a pure Δ excitation. In terms of partial waves this means a predominance of the $^1D_2$ pp partial wave at these energies as is in fact the outcome of the SAID [11] partial wave analysis for the $pp \rightarrow d\pi^+$ reaction. Hence after presentation and discussion of our data we will confront them with theoretical t-channel calculations (Fig.1 , top) as well as with s-channel calculations (Fig. 1, bottom). The latter account for the striking $^1D_2$ partial wave dominance and assume for simplicity that all other partial waves give negligible contributions. In both cases an excitation of the Δ resonance is assumed.

2 Experiment

2.1 Detector setup

Since the experimental setup has been discussed in detail already in (I), we give here only a short account. The measurements have been carried out at the Jülich Cooler Synchrotron COSY using the time-of-flight spectrometer TOF at one of its external beam lines. At the entrance of the detector system the beam - collimated to a diameter smaller than 2 mm - hits the LH$_2$ target, which has a length of 4 mm, a diameter of 6 mm and 0.9 μm thick hostaphan foils as entrance and exit windows. At a distance of 22 mm downstream of the target the two layers of the start detector (each consisting of 1 mm thick scintillators cut into 12 wedge-shaped sectors) were placed followed by a two-plane fiber hodoscope (96 x 96 fibers, 2 mm thick each) at a distance of 165 mm from target. Whereas the start detector mainly supplies the start time signals for the time-of-flight (TOF) measurements, the fiber hodoscope primarily provides a good angular resolution for the detected particle tracks. In its central part the TOF-stop

detector system consists of the so-called Quirl, a 3-layer scintillator system 1081 mm downstream of the target − and in its peripheral part of the so-called Ring, also a 3-layer scintillator system built in a design analogous to the Quirl, however, with inner and outer radii of 560 and 1540 mm, respectively. Finally behind the Quirl a calorimeter was installed for identification of charged particles and of neutrons as well as for measuring the energy of charged particles. The calorimeter consists of 84 hexagon-shaped scintillator blocks of length 450 mm, which suffices to stop deuterons, protons and pions of energies up to 400, 300 and 160 MeV, respectively. The energy calibration of the calorimeter was performed by detecting cosmic muons.

2.2 Particle identification and event reconstruction

In the experiment the trigger required two hits in the Quirl and/or Ring associated with two hits in the start detector. Tracks of charged particles are reconstructed from straight-line fits to the hit detector elements. They are accepted as good tracks, if they originate in the target and have a hit in each detector element the track passes through. In this way the angular resolution is better than $1°$ both in azimuthal and in polar angles. If there is an isolated hit in the calorimeter with no associated hits in the preceding detector elements, then this hit qualifies as a neutron candidate (further criteria will be discussed below). In this case the angular resolution of the neutron track is given by the size of the hit calorimeter block, i.e. by 7 - 8°. By construction of the calorimeter a particle will hit one or more calorimeter blocks. The number of blocks hit by a particular particle is given by the track reconstruction. The total energy deposited by this particle in the calorimeter is then just the (calibrated) sum of energies deposited in all blocks belonging to the particular track.

In order to have maximum angular coverage by the detector elements and to minimize the fraction of charged pions decaying in flight before reaching the stop detectors, the short version of the TOF spectrometer was used. In this way a total polar angle coverage of $3° \leq \Theta^{lab} \leq 49°$ was achieved with the central calorimeter covering the region $3° \leq \Theta^{lab} \leq 28°$. For fast particles the energy resolution of the calorimeter amounting to 4% is superior to that from time-of-flight measurements due to the short path length. However, the time-of-flight resolution is still much better than the ΔE resolution of the Quirl elements. Hence, for particle identification, instead of plotting ΔE versus E_{cal}, the uncorrected particle energy deposited in the calorimeter, we utilize the relation $\Delta E \sim (z/\beta)^2$ with the particle charge $z = 1$ and plot $1/\beta^2$ versus E_{cal}, where the particle velocity $\beta = v/c$ is derived from the time-of-flight measurement.

By identifying and reconstructing the two charged tracks of an event the exit channels $d\pi^+$, $np\pi^+$ and $pp\pi^0$ can be separated. Kinematically the maximum possible laboratory (lab) polar angles are $\approx 9°$ for deuterons and $\approx 32°$ for protons (and neutrons). Hence 86% of the angular coverage for protons and neutrons from single pion produc-

tion are within the angular acceptance of the calorimeter. For charged pions the angular coverage has been much lower with this setup, since kinematically they can extend up to $\Theta^{lab} = 180°$. Hence within the angular coverage of Quirl and Ring the angular acceptance for π^+ has been ≈40% only. Nevertheless most of the phase space part necessary for a full coverage of the physics in single pion production has been covered (see below) by these measurements due to the circumstance that the center-of-mass (cm) angular distributions have to be symmetric about 90° because of identical collision partners in the incident channel.

2.3 Selection of the $np\pi^+$ channel

The $np\pi^+$ channel is selected by identifying proton and pion in the calorimeter or only the proton in the calorimeter, when the second charged track is in the Ring. In addition, the missing $p\pi$ mass $MM_{p\pi}$ has to meet the condition 900 MeV/$c^2 \leq MM_{p\pi} \leq 980$ MeV/c^2 . Also to suppress background from the $d\pi^+$ channel - in particular when the deuteron breaks up and appears as a proton in the calorimeter - the $p\pi^+$ track is required to be noncoplanar. To this end we determine the variable $\Delta\Phi$, which is defined as the projection of the opening angle between two tracks onto the plane normal to the beam vector. That way we have always $\Delta\Phi \leq 180°$. The according histogram is displayed in Fig.2. We see that $p\pi^+$ events stemming from deuteron breakup give rise to a large peak near 180°. In order to get rid of these events we introduce the constraint $\Delta\Phi < 160°$. From Fig. 2 we see that in prinicple a cut $\Delta\Phi < 170°$ would already be sufficient to eliminate this background. However, in order to be on the safe side and to have no perceptible tails from the $pp \to d\pi^+$ reaction in the final data sample, we used the more rigorous constraint. From Fig. 2 we see that this constraint does not cut away significant pieces of physics information [1]. Any extrapolation into the cut region, be it by model or by phase space, will introduce uncertainties on the level of less than two percent.

Aside from this physics background due to deuteron breakup we do not find any sizable background in the final data sample, as has been checked by control measurements, where the target cell was empty.

Further on, the neutron 4-momentum is reconstructed from the 4-momenta of proton and pion and it is checked, whether a calorimeter block in the corresponding (Θ, Φ) region recorded a hit without any additional entries recorded in the preceding detector elements of the Quirl. If these conditions are met, a neutron track is assumed. That way Θ_n and Φ_n are determined by the location of this calorimeter block. By this method we obtain a neutron detection efficiency of 36 %. Thus having only the neutron energy undetermined experimentally we end up with 3 kinematic

---

[1] we note that the data sample with the cut $\Delta\Phi < 170°$ leads to results, which are practically indistinguishable from those shown here

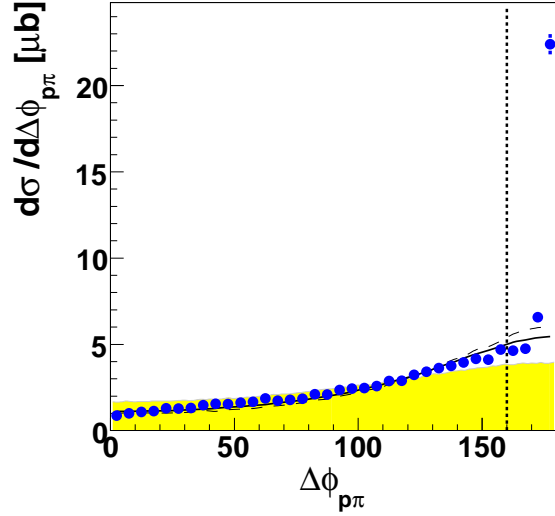**Fig. 2.** Distribution of the planarity angle $\Delta\phi$ defined in the center-of-mass system for the $pp \to pn\pi^+$ reaction. Data of this work are shown by full circles and phase space by the shaded area. Solid and dashed lines denote s-channel and t-channel calculations, respectively, as discussed in the text. For ease of comparison the calculations have been normalized to the experimental total cross section. The constraint $\Delta\Phi < 160°$ for the elimination of events stemming from deuteron breakup is indicated by the vertical dash-dotted line.

overconstraints for this channel. Corresponding kinematic fits were applied.

The luminosity of the experiment was determined from the analysis of pp elastic scattering, see (I). All data have been efficiency corrected by MC simulations of the detector setup by using the CERN GEANT3 [12] detector simulation package, which accounts both for electromagnetic and hadronic interactions of the ejectiles with the detector materials.

2.4 Uncertainties

The final data sample contains about 80000 good events, i.e. the statistical errors are on the percent level and hence of minor importance in comparison with systematical uncertainties. One source of systematic errors are beam alignment and quality. The requirement that the beam has to pass a 2 mm collimator without significant halo assures good alignment and quality of the beam. The alignment is also verified by the fact that the angular distributions in the overall center-of-mass system have to be symmetric about 90 °, see next section. In addition polarized beam measurements with the identical detector setup used here also give no hint for noticeable misalignments [13].

A much more severe source for systematic uncertainties concerns the acceptance and efficiency corrections of

the data. As discussed above the detector covers the complete momentum range , however, not the complete angular range of the reaction of interest. This means, that the acceptance correction has to rely on extrapolations into unmeasured angular regions. From the Dalitz plots displayed in Fig. 4 we see that – according to all we know from this reaction – these unmeasured regions are the ones with the lowest cross section. Hence systematic errors introduced by these extrapolations ought to be of minor importance. To quantify this statement we compare the data resulting from corrections with MC simulations, which are based either on pure phase space or alternatively on a model description of the $pp \rightarrow np\pi^+$ reaction. A model, which is trimmed to describe all essential features of the data, is the appropriate tool for a reliable acceptance and efficiency correction by a MC simulation, which passes the ejectiles from the reaction of interest through the virtual detector. It has the potential of providing a selfconsistent procedure for these corrections. Contrary to this the pure phase space description of the reaction is – as we easily can see from the experimental results displayed in Figs. 2 - 6 – inadequate though convenient. It may serve, however, as a very conservative estimate of the systematic uncertainties due to the acceptance and efficiency corrections. As examples we display in Fig. 3 our data for the invariant pn mass M_{pn} and for the pion angular distribution in the center-of-mass system $\sigma(\Theta_\pi^{CM})$ evaluated (properly) by use of a model, which fits the final data (solid circles), and alternatively by use of pure phase space (open circles), respectively. The use of the latter for the extrapolation into unmeasured regions brings the data, of course, somewhat closer to the phase space predictions. However, despite the fact that phase space and model predictions are vastly different, the effect of the inadequate phase space correction on the data is still very moderate. A realistic upper limit for systematic uncertainties due to acceptance and efficiency correction will be much smaller than the differences between open and solid circles in Fig. 3. As a realistic estimate for this kind of systematic uncertainties we conclude that they are within the size of the symbols, which are used in Figs. 2 - 6 for displaying our experimental results. We note that the use of either t-channel or s-channel calculations in the MC simulations does not lead to any noticeable differences in the acceptance and efficiency corrected data.

3 Results

Due to the identity of the collision partners in the entrance channel the angular distributions in the overall center-of-mass system have to be symmetric about 90 °, i.e. the full information about the reaction channels is contained already in the interval $0° \leq \Theta^{cm} \leq 90°$. Deviations from this symmetry in the data indicate systematic uncertainties in the measurements. Hence we plot - where appropriate - the full angular range, in order to show the absence of major systematic errors in our measurement.

The total cross section of 0.47(2) mb for the $pp \rightarrow pn\pi^+$ reaction at $T_p = 400 MeV$ has already been given
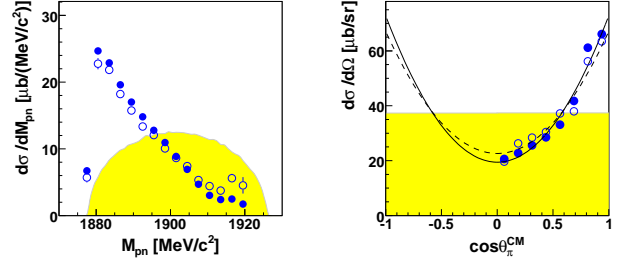

Fig. 3. Differential cross sections in dependence on the invariant mass M_{pn} (left) and the pion scattering angle Θ_π^{CM} (right) in the center-of-mass system for the $pp \rightarrow pn\pi^+$ reaction. The full circles show our data properly corrected by a self-consistent MC simulation, i.e. using a reaction model, which is in agreement with the final data. The open circles derive from MC simulations using just pure phase space. The phase space distributions for the differential spectra are shown by the shaded area. Solid and dashed lines in the right figure show Legendre fits to the filled and open circles yielding $a_2 = 0.96(2)$ and $=0.79(2)$, respectively.

in (I). It is roughly a factor of two smaller than that for the $pp \rightarrow d\pi^+$ channel and five times larger than that for the $pp \rightarrow pp\pi^0$ channel, see Table 1 in (I). For the comparison with data at neighbouring energies [14,3,5,8] see discussion in the next section.

Differential distributions are shown in Figs. 3 - 6. Since a 3-body system in the final state has five independent variables, we choose to present the three invariant mass spectra M_{pn}, $M_{p\pi^+}$ and $M_{n\pi^+}$ as well as the proton and pion angular distributions in the overall center-of-mass system (cms). Because of the limited acceptance for pions only the angular range $0° < \Theta_\pi^{cm} \leq 90°$ is covered. However, as pointed out above, due to the required 90° symmetry of the angular distributions the full information is contained in the data.

In contrast to the $pp\pi^0$ channel the Dalitz plots for the $pn\pi^+$ channel are far from being flat – see Fig.4. This is also borne out in the projections, the invariant mass spectra $M_{p\pi^+}$ and $M_{n\pi^+}$ (see Fig. 5, top), which peak at the highest kinematically available masses. In contrast to these the M_{pn} spectrum (Fig. 5, bottom) peaks at the lowest masses. Note that the high-mass enhancement is similar in both $M_{p\pi^+}$ and $M_{n\pi^+}$ spectra. This is in agreement with the trend observed in bubble chamber data at $T_p = 432$ MeV [4].

Whereas the proton angular distribution is close to flat, the pion angular distribution is strongly anisotropic. It is fitted very well by a pure $(3cos^2\Theta_{\pi^+}^{cm} + 1)$ distribution (solid line in Fig.3, right).

Our results are in good agreement with the results from PROMICE/WASA [6], which are the only other unpolarized data available at $T_p \approx 400$ MeV. Note, however, that those measurements were carried out in a very limited phase space region only. E.g., the pion angular distribution was only measured for $cos(\Theta_{\pi^+}^{cm}) \geq 0.79$.
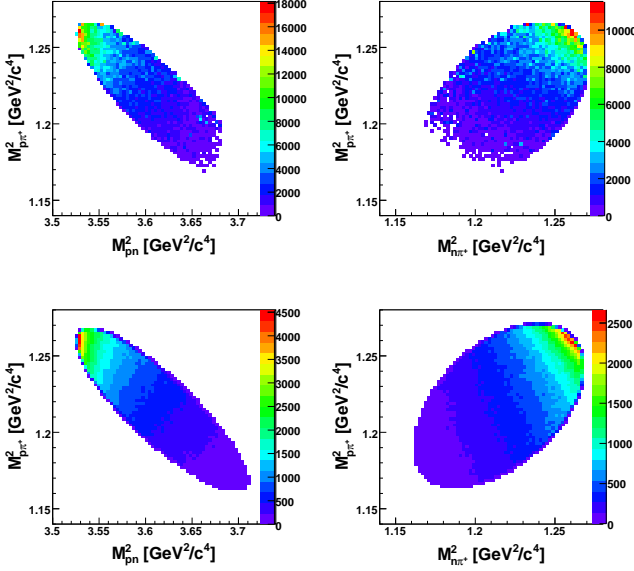
Fig. 4. Dalitz plots for the invariant mass combinations $M^2_{p\pi^+}$ versus M^2_{pn} (left) and $M^2_{p\pi^+}$ versus $M^2_{n\pi^+}$ (right) as obtained for the $pp \to pn\pi^+$ reaction: data are shown on top and the MC s-channel calculation (see text) at the bottom. Note that the plots for the data are efficiency but not acceptance corrected. The tiny deviations from the elliptic circumference at the upper corners are due to the excluded beam-hole region.
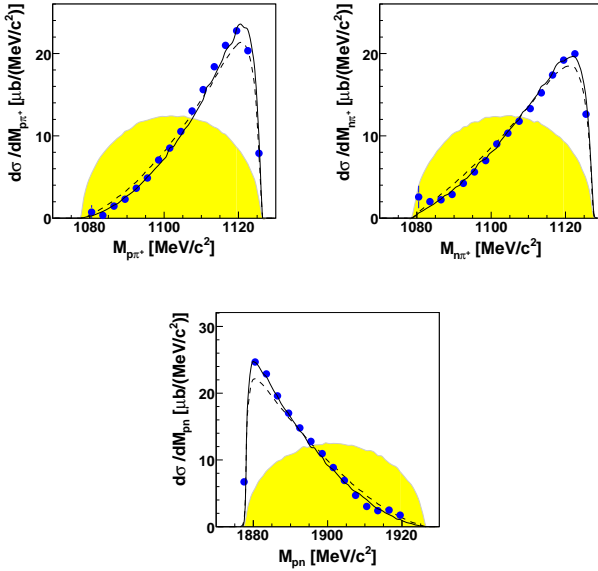

Fig. 5. Differential cross sections in dependence on invariant masses M_{pn}, $M_{p\pi^+}$ and $M_{n\pi^+}$ for the $pp \to pn\pi^+$ reaction. Data of this work are shown by full circles and phase space by the shaded area. Solid and dashed lines denote s-channel and t-channel calculations, respectively, as discussed in the text. For ease of comparison the calculations have been normalized to the experimental total cross section.
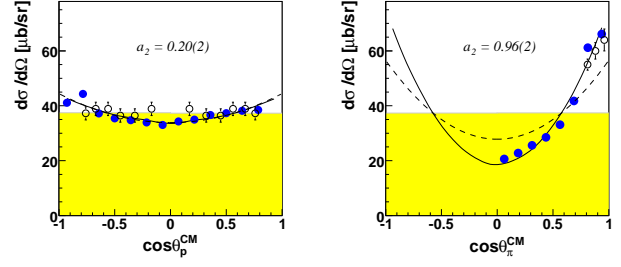

Fig. 6. Angular distributions of protons (left) and pions (right) in the center-of-mass system for the $pp \to pn\pi^+$ reaction. Data of this work are shown by full circles, WASA/PROMICE results [6] by open circles (renormalized to σ_{tot} of this work) and phase space by the shaded area. Solid and dashed lines denote s-channel and t-channel calculations, respectively, as discussed in the text. For ease of comparison the calculations have been normalized to the experimental total cross section. Given are also the Legendre coefficients a_2 from a Legendre fit according to eq. 2 in (I) tgether with statistical errors.
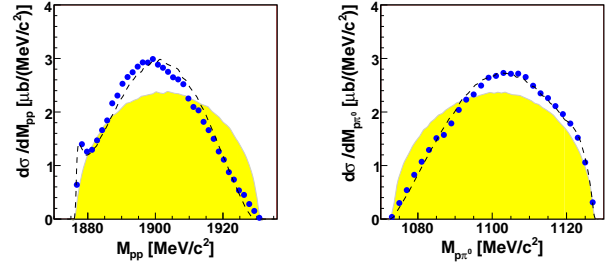

Fig. 7. Differential cross sections in dependence on invariant masses M_{pp} (left) and $M_{p\pi^0}$ (right) for the $pp \to pp\pi^0$ reaction (from (I)). Phase space is shown by the shaded area. For the explanation of the curves see (I).

4 Discussion of Results

4.1 Comparison with the $pp\pi^0$ channel

For the comparison of $pn\pi^+$ and $pp\pi^0$ channels we show once more results in Figs. 7 and 8, which we obtained previously for the $pp\pi^0$ channel, see (I).

The proton angular distributions both in $pn\pi^+$ and $pp\pi^0$ channels are close to isotropic (see Figs. 6 and 8, left). They nevertheless show a tendency of opposite curvature, which just may be some reflection of the very different pion angular distributions in both channels. At these low energies the pion angular distributions are described conveniently by the Legendre ansatz

$$\sigma(\Theta^{cm}_{\pi^0}) \sim 1 + a_2 * (3cos^2\theta^{cm}_{\pi^0} - 1)/2,$$

where the parameter a_2 is fitted to the data. This ansatz has also been used in (I) for the analysis of the $pp\pi^0$ channel – see eq. 2 in (I). Other notations related to our a_2 parameter are as follows: in the notation of Ref. [5], Table III we have $a_2 = A_2/A_0$, in the notation of Ref.
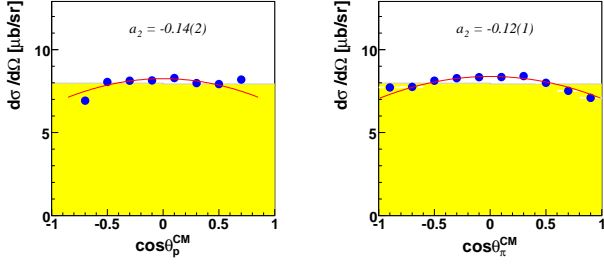
Fig. 8. Angular distributions of protons (left) and pions (right) in the center-of-mass system for the $pp \to pp\pi^0$ reaction (from (I)). The solid curves represent Legendre fits, see (I).

[8], Table V we have $a_2 = B/A$ and in the notation of Ref. [10], Table II we have $a_2 = 2*b_{00}$ (since $a_{00} = 1$ there).

For the pion angular distribution in case of $pp\pi^0$ we find a slightly concave shape (Fig. 8, right; $a_2 = -0.12$), whereas we get a strongly convex shape in case of the $pn\pi^+$ channel (Fig. 6, right; $a_2 = +0.96(2)$).

A striking difference to the $pp\pi^0$ channel is the dominance of the Δ excitation in the $pn\pi^+$ channel. In the $pp\pi^0$ channel Δ production in a s-wave relative to the accompanying nucleon is prohibited by quantum numbers. However, as demonstrated in (I), the Δ production in relative p-wave is allowed and indeed contributes significantly to this channel already close to threshold.

The signature of Δ production in the $pn\pi^+$ channel is seen in all differential observables shown in Figs. 3 - 6. The M_{pn} spectrum (Fig. 5, bottom) is markedly different from the M_{pp} spectrum in the $pp\pi^0$ channel (Fig. 7, left). Though the pn final state interaction (FSI) is somewhat larger than the pp FSI, it cannot account for the huge difference between both spectra at low masses. It rather is a reflection from the complementary spectra $M_{p\pi^+}$ and $M_{n\pi^+}$, which peak just at the highest available masses (Fig. 5, top) in contrast to the more phase-space like $M_{p\pi^0}$ spectrum observed in the $pp\pi^0$ channel (Fig. 7, right). The high-mass enhancement in turn is most likely associated with Δ excitation.

4.2 Pion angular distribution

The most striking feature in our $pn\pi^+$ data at $T_p = 400$ MeV is the $(3\,cos^2\Theta_{\pi^+}^{cm} + 1)$ dependence of the pion angular distribution. It is exactly this dependence, which is seen in πN scattering in the Δ resonance region and which is also observed in the $pp \to d\pi^+$ reaction over a large range of incident energies. We note that also the pion angular distributions at $T_p = 420$ and 500 MeV, deduced from inclusive measurements of the $pp \to pn\pi^+$ reaction in Ref. [5] are basically in accord with this dependence.

We also note in passing, that in contrast to the situation in the $pp\pi^0$ channel, where we observe a strong dependence of the pion angular distribution on the relative momentum q between the two nucleons in the exit

channel, we do not find such a behavior here. The pion angular distributions stay essentially the same for different q-regions. This again is in support of a single dominant mechanism proceeding via a single partial wave.

Whereas we find good agreement in the anisotropy of the pion angular distribution with the ones measured at TRIUMF at $T_p = 420$ and 500 MeV [5], we face a profound discrepancy with IUCF results [10]. There kinematically complete measurements with both polarized beam and target are presented for $T_p = 325$, 350, 375 and 400 MeV together with Legendre polynomial fits, which reproduce the measured angular distributions of the polarization observables. In Table II of Ref. [10] the coefficients resulting from these fits are listed. This list also contains the anisotropy parameter $b_{00} = a_2/2$ for the unpolarized differential cross section $\sigma(\Theta_\pi^{CM})$. Since that paper concentrates on the polarization observables, it does not discuss the unpolarized $\sigma(\Theta_\pi^{CM})$ data in any detail. It is just noted that these have been deduced from $p + n$ coincidences. As a result of their Legendre analysis they obtain $a_2 = 0.39\,(9)$ for $T_p = 400$ MeV, a value, which is less than half of our value. The difference amounts to six standard deviations. We face here perhaps a similar problem as discussed in (I) for the situation of the experimental data with the reaction $pp \to pp\pi^0$ at the same beam energy of $T_p = 400$ MeV. There also a large discrepancy exists between the asymmetry parameter a_2 found in the IUCF analysis and the one we found at COSY-TOF. Our result has meanwhile been confirmed by CELSIUS/WASA data [15]. In both these works it has been shown that previous results – like the one obtained at PROMICE/WASA [16] – suffered from insufficient phase space coverage combined with inappropriate extrapolations into the unmeasured regions.

We note the following surprising trend in the results of the IUCF analyses concerning the a_2 parameter. In agreement with previous IUCF work very close to threshold [8], where a strong increase in the a_2 value with energy is observed ($a_2 = 0$, 0.12 and 0.31 at $T_p = 294$, 299 and 319 MeV, respectively), a value of $a_2 = 0.34(7)$ at $T_p = 325$ MeV is reported in Ref. [10], Table II. This increase just reflects the increasing importance of the Δ excitation in the $pp \to np\pi^+$ reaction. However, above $T_p = 325$ MeV Ref. [10](see again Table II) finds that the a_2 parameter no longer increases, but rather saturates at a value of 0.39. This implies that the Δ contribution also suddenly saturates despite the fact the Δ pole is still far from being reached at these energies. Also the Jülich model calculations [17], which are used in Ref. [10] for comparison with the polarization data predict a strongly increasing importance of the Δ excitation at these beam energies – as also expected intuitively.

In Ref. [10] the discrepancy between their 400 MeV result and the TRIUMF data at $T_p = 420$ MeV [5] was not discussed. The TRIUMF measurements were performed as a single-arm experiment with a magnetic spectrometer, which measures a 3-body reaction only inclusively. Such measurements are known to be very reliable for the determination of single-particle angular distributions, since

exactly the same detector is used for the particle detection at all angles minimizing thus the problem of acceptance and efficiency corrections.

To summarize the discussion about a_2 we face a severe discrepancy between the IUCF and COSY-TOF results at $T_p = 400$ MeV for both the $pp \rightarrow pp\pi^0$ reaction and the $pp \rightarrow np\pi^+$ reaction. However, there is good agreement of our result for the first reaction with the corresponding one from CELSIUS/WASA and for the second reaction with the one obtained at TRIUMF. We finally note that the uncertainty of a_2 quoted in Fig.6 only includes the statistical uncertainties of the data. If we include an estimate on systematic uncertainties (as discussed above in the section 2.4), we end up with an estimated total uncertainty of $\Delta a_2 \approx 0.08$.

The close similarity in the angular distributions of $d\pi^+$ and $pn\pi^+$ channels is in agreement with the predictions of Fäldt and Wilkin [18], according to which the meson angular distributions coincide closely in bound state and breakup channels near threshold.

The $(3 \cos^2\Theta_{\pi^+}^{cm} + 1)$ dependence in the $pp \rightarrow d\pi^+$ reaction is due to the $^1D_2$ partial wave in the incident pp channel combined with the constraint of a p-wave pion relative to the deuteron in the exit channel. As known from phase shift analyses of this reaction [11,19] this ^1D_2P partial wave dominates the $pp \rightarrow d\pi^+$ reaction basically from threshold up to $T_p \approx 900$ MeV. It is responsible for the resonance-like energy dependence of the total cross section and performs a perfect looping in the Argand diagram [11]. Thus this partial wave possesses all features to qualify for a s-channel resonance with $I(J^P) = 1(2^+)$ in the incident pp channel, the final $d\pi^+$ channel and the intermediate $N\Delta$ channel – see also discussion in Ref. [27]. From the total cross section of the ^1D_2P partial wave in the $pp \rightarrow d\pi^+$ reaction [11] we see that the resonance energy is some 60 MeV below the nominal $N\Delta$ threshold, whereas the resonance width of ≈ 110 MeV corresponds to that of the Δ resonance.

The experimental observation that up to $T_p = 500$ MeV essentially a $(3 \cos^2\Theta_{\pi^+}^{cm} + 1)$ dependence is observed also in the $pp \rightarrow pn\pi^+$ reaction points to the predominance of the ^1D_2P partial wave in this reaction, too, as was already noted in Ref. [5]. From this also follows that the pn system at these energies is preferably in the deuteron-like quantum state $I(J^P) = 0(1^+)$.

4.3 Total cross section

The energy dependence of the total cross sections for the $pp \rightarrow d\pi^+$ and $pp \rightarrow np\pi^+$ channels is displayed in Fig. 9. For the $pp \rightarrow pn\pi^+$ channel at $T_p = 400$ MeV there are no experimental data to compare with. However, our result fits well to the trend given by the experimental results [14,3,5,8] at neighbouring energies. In order to discuss in the next section the energy dependence in some broader context with regard to the dominance of the $^1D_2$ partial wave, we plot in Fig.9 the energy range from threshold up to $T_p = 1.5$ GeV, i.e. over the full region of Δ excitation.
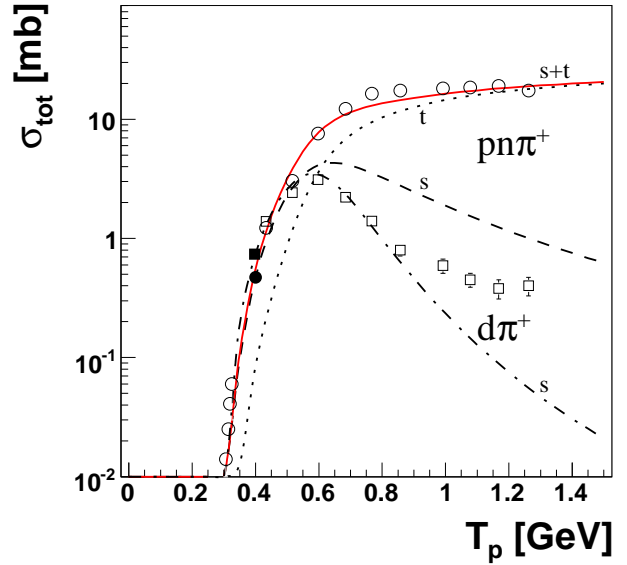

Fig. 9. Energy dependence of total cross sections for the reactions $pp \rightarrow d\pi^+$ (squares) and $pp \rightarrow pn\pi^+$ (circles). The filled symbols denote results of this work, open symbols are from [14, 3,8]. Dash-dotted and dashed lines represent s-channel calculations for $d\pi^+$ and $pn\pi^+$ channels, respectively, normalized to the data at $T_p = 400$ MeV. The t-channel calculation for the $pn\pi^+$ channel is given by the dotted line and normalized to the data at $T_p \geq 1$ GeV, where it is known to provide a reasonable description. The solid curve denoted by s + t is the incoherent sum of both processes for the $pp \rightarrow pn\pi^+$ channel.

4.4 Comparison to t- and s-channel calculations

Finally we confront the data with simple theoretical calculations according to the graphs depicted in Fig. 1. In this experimental paper it is not our aim to compare our data with complex calculations, which are beyond the scope of this work. We rather want to use these calculations in order extract the main physics message residing in the data.

Since we have seen in the discussion above that Δ excitation and decay is the dominant reaction mechanism and $^1D_2$ is by far the dominant partial wave at least in the energy region $T_p = 400$ - 500 MeV, we explicitly neglect any non-resonant terms in the reaction process.

We start with a (properly antisymmetrized) t-channel approach in first-order impulse approximation, which is known to provide reasonable results for the angular distributions at energies $T_p \geq 1$ GeV [20,21,22,23,24]. For our energy we show such a t-channel calculation by the dashed lines in Figs. 2, 3, 5 and 6. We see that the pion angular distribution is not reproduced correctly. The reason for this failure is simple. Since in this approach the Δ is excited by pion exchange between the two colliding nucleons, the reference axis for the pion decay of the excited Δ resonance is the momentum transfer $\mathbf{q}$ and not the beam axis. Note that the latter, however, is the reference axis
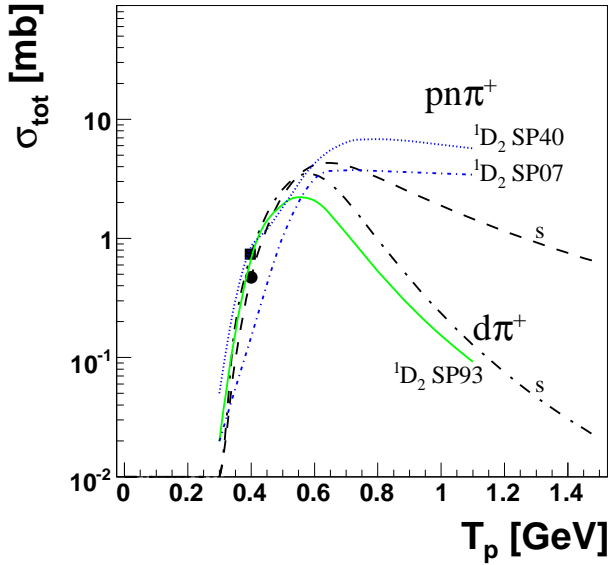
Fig. 10. Energy dependence of total cross sections as calculated with our s-channel approach for the $pp \to d\pi^+$ (dash-dotted) and $pp \to pn\pi^+$ (dashed cureve) reactions, normalized to the data points from this experiment at $T_p = 400$ MeV (filled square and circle, respectively; see also Fig. 9). For comparison the short dash-dotted and dotted lines give the SAID [11] solutions SP07 and SP40, respectively, for the $^1D_2$ partial wave in the $np\pi^+$ channel (see text), whereas the solid curve shows the SAID solution SP93 for the $^1D_2$ partial wave in the $d\pi^+$ channel.

for angles in the center-of-mass frame. Since the momentum transfer varies in dependence of the nucleon scattering angles, which are integrated over in the pion angular distribution, the calculated intrinsic $(3 \cos^2\Theta_{\pi^+}^q + 1)$ dependence in the t-channel approach appears to be smeared out in the cms pion angular distribution.

In order to establish the beam direction as the appropriate reference axis for the pion angular distribution in the calculation one either has to reiterate the pion exchanges and sum them up to infinity or simply make a s-channel ansatz. The latter is easily made by a Breit-Wigner ansatz for the $^1D_2$ resonance (Fig. 1, bottom), which dissociates into a $N\Delta$ system in relative s-wave followed by the decay of the Δ resonance. This grants the observed $(3 \cos^2\Theta_{\pi^+}^{cm} + 1)$ dependence for the pions as well as the desired shape of the invariant mass spectra. To simulate the $pp \to d\pi^+$ reaction within this ansatz we impose the Hulthen wave function as condition for the Fermi momentum between proton and neutron. For the $pp \to pn\pi^+$ reaction we impose a FSI interaction of Migdal-Watson type [25,26] on the pn system. These calculations (normalized to our results for the total cross sections at $T_p = 400$ MeV) are shown by the Dalitz plots in Fig. 4, bottom and by the solid lines in Figs. 2,3, 5 and 6. They give a

good account of the differential distributions both for the invariant masses and for the particle emission angles.

Mass (2.07 GeV) and width (160 MeV) of the $I(J^P) = 1(2^+)$ resonance in this s-channel ansatz have been chosen to reproduce the energy dependence of the total cross section of the $pp \to d\pi^+$ reaction in the region of the ^1D_2P dominance, i.e. up to $T_p \approx 700$ MeV. That way we simultaneously get a good description for the energy dependence of the total cross section for the $pp \to pn\pi^+$ reaction up to $T_p \approx 600$ MeV. If combined with the amplitude of the t-channel approach we even obtain a reasonable description of the total cross sections up to the GeV region (Fig. 9).

Finally we compare in Fig. 10 our simple s-channel calculations for the $^1D_2$ partial wave in the $np\pi^+$ channel to the results of SAID [11] partial wave analyses of NN scattering and $pp \to d\pi^+$ reaction. The imaginary part of the $^1D_2$ partial wave, which is obtained from the analysis of elastic NN scattering, gives rise to the total inelastic cross section $\sigma_{inel}(^1D_2)$ for the $^1D_2$ partial wave, which in turn is given by the sum of the pion-production cross sections in this partial wave. Since in the $pp \to pp\pi^0$ reaction the $^1D_2$ partial wave is highly suppressed due to the suppression of the Δ excitation, we have in good approximation

$$\sigma_{pp \to np\pi^+}(^1D_2) \approx \sigma_{inel}(^1D_2) - \sigma_{pp \to d\pi^+}(^1D_2)$$

The thus derived results are shown in Fig. 10 for the SAID solutions SP07 and SP40 from NN scattering analyses together with the SAID solution SP93 for the $^1D_2$ partial wave in the $d\pi^+$ channel. We see that our s-channel ansatz overpredicts the $^1D_2$ part of the $pp \to d\pi^+$ cross section at higher energies as expected, since we have assumed for simplicity that only this partial wave contributes. For the $np\pi^+$ channel the SP07 solution underpredicts the cross section in the near-threshold region strongly, whereas the SP40 solution, which is made for the region $T_p \le 400$ MeV, provides a proper energy dependence, however, is in the absolute scale substantially above the data and the s-channel calculation in this energy region. At higher energies up to 800 MeV our calculation is essentially between both solutions. This comparison with the SAID solutions for the $^1D_2$ partial wave shows that our simple model description is not in severe contradiction to the SAID results, where the large spread between both solutions points to still substantial ambiguities in the NN partial wave analyses concerning the imaginary parts of partial waves.

5 Summary

We have presented measurements of the $pp \to pn\pi^+$ reaction at $T_p \approx 400$ MeV. In this energy region they are the first exclusive ones of solid statistics to cover most of the reaction phase space. The differential distributions are characterized by the overwhelming dominance of the Δ excitation. The pion angular distribution coincides with that observed in the $pp \to d\pi^+$ channel, which in turn is dominated by the resonating ^1D_2P partial wave. From this coincidence we conclude that also the $pn\pi^+$ channel

is dominated by the same s-channel resonance in the near-threshold region. The correlation between boundstate and breakup channels is in accordance with the predictions by Fäldt and Wilkin [18].

References

1. S. Abd El-Samad et al., Eur. Phys. J. **A30**, 443 (2006)
2. B. Neganov, O. Savchenko, Sov. Phys. JETP **5**, 1033 (1957)
3. F. Shimizu et al., Nucl. Phys. **A386**, 571 (1982)
4. F. Shimizu et al., Nucl. Phys. **A389**, 445 (1982)
5. R. G. Pleydon et al., Phys. Rev. **C59**, 3208 (1999)
6. A. Betsch et al., Phys. Lett. **B446**, 179 (1999)
7. W. W. Daehnick et al., Phys. Rev. Lett. **74**, 2913 (1995)
8. J. G. Hardie et al., Phys. Rev. **C56**, 20 (1997)
9. R. W.Flammang et al., Phys. Rev. **C58**, 916 (1998), Phys. Rev. **C60**, 029901 (1999)
10. W. Daehnick et al., Phys. Rev. **C65**, 024003 (2002)
11. R. A. Arndt et al., Phys. Rev. **C48**, 1926 (1993); SAID data base see also http://said.phys.vt.edu
12. GEANT3, version 3.21, CERN Computing and Networks Divison, *GEANT - Detector description and Simulation Tool*, CERN Program Library
13. S. Abd El-Bary et al., Eur. Phys. J. **A37**, 267 (2008); arXiv:0806.3870 [nucl-ex]
14. for a data compilation see J. Bystricky et al., J. Physique **48**, 1901 (1987); database HEPDATA, Durham University http://durpdg.dur.ac.uk/hepdata/reac.html; IHEP cross sections database http://wwwppds.ihep.su:8001/acs.htm
15. P.Thörngren Engblom et al., Phys. Rev. **C76**, 011602(R) (2007)
16. R. Bilger et al., Nucl. Phys. **A693**, 633 (2001)
17. C. Hanhart et al., Phys. Rev. **C61**, 064008 (2000), Phys. Rep. **397**, 155 (2004)
18. G. Fäldt and C. Wilkin, Phys. Lett. **B382**, 209 (1996) and **B389**, 440 (1996)
19. R. A. Arndt, Phys. Rev. **165**, 1834 (1968)
20. V. Dmitriev, O. Sushkov, C. Gaarde, Nucl. Phys. **A459**, 503 (1986)
21. S. Huber, J. Aichelin, Nucl. Phys. **A573**, 587 (1994)
22. P. Fernandez et al., Nucl. Phys. **A586**, 586 (1995)
23. S. Teis et al., Z. Phys. **A356**, 421 (1997)
24. V. Sarantsev et al., Eur. Phys. J. **A21**, 303 (2004)
25. A. B. Migdal, J. Exp. Theor.Phys. **28**, 1 (1955)
26. K. W. Watson, Phys. Rev. **88**, 163 (1952)
27. H. Clement et al., Prog. Part. Nucl. Phys. **61**, 276 (2008); arXiv: 0712.4125 [nucl-ex]